Jurnal Teknologi

Full Paper

PHYSICAL, MECHANICAL, MORPHOLOGICAL AND THERMAL ANALYSIS OF STYRENE-CO-GLYCIDYL METHACRYLATE / FUMED SILICA / CLAY NANOCOMPOSITES

Josephine Chang Hui Lai[a*], Md. Rezaur Rahman[a], Sinin Hamdan[b]

[a]Department of Chemical Engineering and Energy Sustainability, Faculty of Engineering, Universiti Malaysia Sarawak (UNIMAS), 94300 Kota Samarahan, Sarawak, Malaysia
[b]Department of Mechanical and Manufacturing Engineering, Faculty of Engineering, Universiti Malaysia Sarawak (UNIMAS), 94300 Kota Samarahan, Sarawak, Malaysia

Article history
Received
21 November 2016
Received in revised form
12 April 2017
Accepted
31 May 2017

*Corresponding author
lchjosephine@unimas.my

Graphical abstract

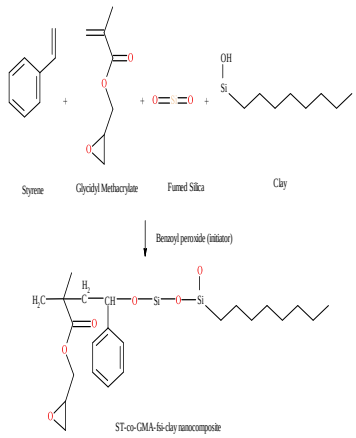

Abstract

Styrene-co-glycidyl methacrylate-fumed silica-clay (ST-co-GMA-fsi-clay) nanocomposites have been prepared via free radical polymerization in the presence of benzoyl peroxide. The nanocomposites are characterized by Fourier transform infrared spectroscopy (FT-IR), scanning electron microscopy (SEM), adsorption isotherm, tensile test, thermogravimetric analysis (TGA) and moisture absorption. FT-IR shows the Si-O-C peak that represented ST-co-GMA-fsi bonding while Si-O-Si peak shows the bonding of fsi-clay. The surface morphology shows the well dispersion of clay (1.30E) into ST-co-GMA-fsi nanocomposite. 2wt% of ST-co-GMA-fsi-clay (1.30E) nanocomposite has higher specific surface area and average pore volume with less pore size. Incorporation of 2wt% of clay (1.30E) improves the tensile strength and modulus of the nanocomposites as well as higher thermal stability and activation energy. 2wt% of ST-co-GMA-fsi-clay (1.30E) nanocomposite shows the lowest moisture absorption value.

Keywords: Adsorption, morphology, TGA, clay, nanocomposites

Abstrak

Stirena bersama glycidyl metakrilat-silika berwap-tanah liat (ST-co-GMA-fsi-tanah liat) nanokomposit telah disediakan melalui pempolimeran radikal bebas dengan kehadiran benzoyl peroksida. Nanokomposit melalui ciri-ciri jelmaan Fourier spektroskopi inframerah (FT-IR), imbasan mikroskop electron (SEM), penjerapan isoterma, ujian tegangan, analisis Termogravimetri (TGA) dan peyerapan kelembapan. FT-IR menunjukkan puncak Si-O-C yang mewakili ikatan ST-co-GMA-fsi manakala Si-O-Si puncak menunjukkan ikatan silika berwap-tanah liat. Morfologi permukaan menunjukkan penyebaran perigi tanah liat (1.30E) ke dalam ST-co-GMA-silika berwap nanokomposit. 2wt% daripada ST-co-GMA-silika berwap-tanah liat (1.30E) nanokomposit mempunyai kawasan permukaan lebih tinggi khusus and purata isi padu liang dengan kurang saiz liang. Pemerbadanan 2wt% daripada tanah liat (1.30E) meningkatkan kekuatan tegangan dan modulus dan juga kestabilan terma bersama dengang tenaga pengaktifan yang tinggi. 2wt% daripada ST-co-GMA-silika berwap-tanah liat (1.30E) nanokomposit menunjukkan nilai penyerapan kelembapan yang paling rendah.

Kata kunci: Penjerapan, morfologi, TGA, tanah liat, nanokomposit

1.0 INTRODUCTION

Polymer matrix has been widely used as matrix for composites production. Most of the polymer matrices have great properties that include excellent toughness and adhesion. Some of these resins undergo ring opening when reacted with substances possess methylene groups [1].

Styrene (ST) is a monomer that helps to enhance the rigidity of the copolymer [2]. Styrene is prepared through the dispersion polymerization, suspension polymerization, bulk polymerization, atom transfer radical polymerization (ATRP) and radical emulsion polymerization [3]. Styrene-based composites can be applied in the automotive fields [4].

Glycidyl methacrylate (GMA) is another monomer that has flexible applications. They are commercially available vinyl monomer carrying epoxy group. GMA is useful for polymer matrix modification that can be utilized as matrix for drug delivery [5]. Benzoyl peroxide is used as initiator for styrene-based copolymer or GMA-based copolymer [6].

ST-co-GMA does not possess adequate thermal and mechanical properties due to low melting temperature. Therefore, nanofiller such as fumed silica and nanoclay was incorporated to overcome this problem. Inorganic fumed silica acted as nanofiller is usually incorporated into polymer matrix to enhance the interfacial area as well as the mechanical properties of the nanocomposites. It is widely used due to their high surface area [7].

Clay is nanofiller that can be introduced into polymer nanocomposites. It is layered structure that consists of an octahedral alumina sheet stacked between two tetrahedral silica sheets by a weak dipolar force leads to interlayer galleries [8]. Clay is widely used due to its low cost, high availability and environmental friendly. The most common used clay is montmorillonite. It can be applied in many applications such as construction, polymer and medicine industries [9].

It was confirmed that the compatibility of fumed silica improved ST-co-GMA by reducing the agglomerate formed. The incorporation of fumed silica in ST-co-GMA had improved the mechanical properties due to the covalent bonds between the epoxy groups of ST-co-GMA and silanol groups from silica increased the filler-matrix interaction [10]. Fumed silica was incorporated into styrene matrix that had enhanced the tensile strength and heat resistance [11]. Polystyrene-fumed silica undergo free radical polymerization that had enhanced the tensile strength due to the high dispersion and excellent compatibility between the polymer matrix and filler [12]. The incorporation of fumed silica onto poly(GMA) matrix had enhanced thermal stability of the nanocomposites. The FT-IR spectroscopy showed that poly(GMA) was well intercalated with fumed silica nanoparticle by free radical polymerization [13].

Silica was well dispersed in the styrene matrix that enhanced the compatibility within the composites [14]. Lower percentage of clay improved the thermal stability of ST-co-GMA compared to higher percentage of clay. The intercalation of clay into polystyrene matrix improved the tensile strength through melt intercalation. Poly(GMA)-clay nanocomposites undergo free radical in situ polymerization that had enhanced thermal and mechanical performances compared to epoxy-bentonite nanocomposites [15].

The introduction of dual fillers such as fuemd silica with the fibers into styrene-butadiene copolymers improved the mechanical properties of the composites [16]. Besides, wood styrene acrylonitrile was impregnated with fumed silica and nanoclay as the nanofillers improved the hardness of the nanocomposites [17].

Single filler onto styrene or glycidyl methacrylate-based nanocomposites had improved the mechanical and thermal properties significantly. However, the surface morphology and physical properties did not significantly improved by single filler loaded nanocomposites. To overcome the above mentioned drawback, the present study investigated dual filler loadings on ST-co-GMA and their compatibility. Dual fillers were used as clay can improved the interfacial adhesion which led to better morphological properties while fumed silica could improved the thermal properties [8, 11]. Therefore, dual fillers managed to improve all the properties simultaneously onto the polymer matrix. The physical, morphological, mechanical and thermal properties of ST-GMA-fsi-clay (1.30E) were also reported in this study. The novely of this nanocomposite is expected to be applied as construction materials in building industry. This is because the weak interfacial bonding between polymer matrix allows the fillers (fumed silica and clays) particles to be introduced and created better interfacial bonding that improved the mechanical and thermal properties and it can be well applied for inner and exterior purposes [18].

2.0 METHODOLOGY

2.1 Materials

Styrene, glycidyl methacrylate and benzoyl peroxide were supplied by Merck, Germany. Benzoyl peroxide acted as an initiator to influence the reaction between styrene and glycidyl-methacrylate. Fumed silica powder with particle size less than 8 microns in white colour was used as filler in the preparation of nanocomposites. Nanomer 1.30E was montmorillonite clay modified with 25-30wt% octadecylamine used as nanofiller. The bulk density of nanoclay was 200 to 500 kg/m3 and the average particle size was around 20 microns. The clay and silicon dioxide powders were supplied by Sigma-Aldrich, USA.

2.2 Free Radical Polymerization of ST-co-GMA-fsi-clay Nanocomposites

The polymer nanocomposite was prepared using styrene, glycidyl methacrylate, fumed silica and clay (1.30E) in four weight percentages in the presence of benzoyl peroxide. The composition of nanocomposites was prepared as shown in Table 1.

50mL of styrene, 50mL of glycidyl methacrylate, 0.2g of fumed silica powder and different clay loadings (1.0g, 2.0g, 3.0g and 4.0g) were placed in a 500mL beaker in the presence of benzoyl peroxide. The mixture was heated for 10 minutes in an heater at 80°C. The mixture was then cast on a glass surface and kept in a desiccator for controlled evaporation of the solvent for a day. The optically clear nanocomposite films with thickness ranging from 500 to 700 µm were obtained and were kept in desiccator for further characterizations and analysis. The samples were named as ST-co-GMA (SG), ST-co-GMA-fsi (SGFSN), 1wt% ST-co-GMA-fsi nanocomposites (SGFSCN1), 2wt% ST-co-GMA-fsi nanocomposites (SGFSCN2), 3wt% ST-co-GMA-fsi nanocomposites (SGFSCN3) and 4wt% ST-co-GMA-fsi nanocomposites (SGFSCN4).

Table 1 Preparation of ST-co-GMA-fsi composites system with different types of clay loading

Amount of styrene (mL)	Amount of glycidyl methacrylate (mL)	Amount of benzoyl peroxide (g)	Amount of fumed silica (g)	Amount of clay (g)
50	50	2	-	- SG
50	50	2	0.2	- SGFSN
50	50	2	0.2	1.0 (1wt%) SGFSCN1
50	50	2	0.2	2.0 (2wt%) SGFSCN2
50	50	2	0.2	3.0 (3wt%) SGFSCN3
50	50	2	0.2	4.0 (4wt%) SGFSCN4

2.3. Characterization of ST-co-GMA-fsi-clay Nanocomposites

2.3.1 Fourier Transform Infrared Spectroscopy (FT-IR)

The infrared spectra of the nanocomposites were recorded on a Shimadzu IRAffinity-1. The transmittance range of the scan was 4000 to 700cm^{-1} [19].

2.3.2 Scanning Electron Microscopy (SEM)

The interfacial bonding between the styrene, glycidyl methacrylate, fumed silica and clay (1.30E) was examined using a scanning electron microscope (SEM) (JSM-6710F) from JEOL Company Limited, Japan. The specimens were first fixed with Karnovsky's fixative and then take through a graded alcohol dehydration series. Once dehydrated, the specimen was coated with a thin layer of gold before being viewed microscopically. The micrographs were taken at magnifications ranging from 500x to 1000x [19].

2.3.3 Adsorption Isotherm

The nitrogen adsorption isotherms of ST-co-GMA, ST-co-GMA-fsi and ST-co-GMA-fsi-clay (1.30E) nanocomposites at 77K were obtained by using a Quantachrome, Asic-7 physicosorption analyzer. In this analysis, the nanocomposites were degassed at 250°C in vacuum for an hour before the nitrogen adsorption isotherm was constructed. The surface area and pore volume of nanocomposites were evaluated by the Brunauer-Emmett-Teller (BET) model [19].

2.3.4 Tensile Test

Thin films were cut with a rectangular die and tested with AG-Xplus Series Precision Universal Testers (300kN Floor Model) supplied by Shimadzu Corporation at room temperature. The gauge length, width and thickness of the samples were 25, 4 and 0.15mm respectively. The cross head speed used was 1mm/min. The quoted results were averaged over ten specimens [19].

2.3.5 Thermogravimetric Analysis (TGA)

Thermogravimetric analysis (TGA) measurements were carried out on 5-10mg of ST-co-GMA, ST-co-GMA-fsi and ST-co-GMA-fsi-clay (1.30E) nanocomposites at a heating rate of 10°C/min in a nitrogen atmosphere using a Thermogravimetric Analyzer (TA Instrument SDT Q600). ST-co-GMA, ST-co-GMA-fsi and ST-co-GMA-fsi-clay (1.30E) nanocomposites were subjected to TGA in high purity nitrogen under a constant flow rate of 5mL/min. Thermal decomposition of each sample occurred in a programmed temperature range of 20°C to 700°C. The continuous weight loss and temperature were recorded and analyzed [19].

2.3.6 Moisture Absorption

The moisture absorption was carried out at 110°C for 3h by using electronic moisture balance (MOC-120H) supplied by Shimadzu Corporation, Kyoto, Japan. Dry nanocomposites (dried at 25°C) were immersed in distilled water, continued by removing and weighing process. The nanocomposites were placed in flat

position into the tester during the measurement. The heater lid was then been closed firmly and the display switched from a display of the weight to a percentage display and the measuring time was displayed too. The moisture absorbed, Wab was calculated by using Eq. (1) [19].

Moisture absorbed percentage, Wab (%) = [(weight of wet nanocomposites (W_w)-(weight of dry nanocomposites (W_d))/(weight of wet nanocomposites (W_w)x100 Eq. (1)

3.0 RESULTS AND DISCUSSION

3.1 Fourier transform infrared spectroscopy (FT-IR)

The FT-IR spectra of the ST-co-GMA, ST-co-GMA-fsi and ST-co-GMA-fsi-clay (1.30E) nanocomposites were shown in Figure 1. The spectra confirmed the presence of the functional groups in ST-co-GMA-fsi-clay (1.30E) nanocomposites with the chemical reaction as shown in Figure 2.

The absorption peak at 3350cm^{-1} represented the O-H stretching vibration within the GMA monomer as shown in Figure 1(a-b). The C-H stretching vibration was detected at 2970cm^{-1} in all the samples [20]. However, the intensity of the peak at 2wt% of clay loaded ST-co-GMA-fsi-clay (1.30E) nanocomposite was broader because of the optimum loading. The peak intensity decreased was attributed to the pore filling effects of clay at the maximum loading of 2wt% which could reduce the scattering contrast between the pores and improved the interfacial bonding within the nanocomposite formed. [21]. The existence of ST-co-GMA could be proven with the appearance of absorption peak at 1725cm^{-1} which corresponded to the carbonyl group vibration in all the samples [1]. It was detected that the peak at 1664cm^{-1} attributed to the deformation vibration in the H-O-H groups [22]. This peak was significant when 1wt% and 2wt% of clay (1.30E) was introduced into the ST-co-GMA-fsi nanocomposites as shown in Figure 1(c-d). The C=C double bond from styrene with GMA was indicated by the absorption peak at 1600cm^{-1} [1].

In addition, the absorption peak at 1465cm^{-1} was attributed to the vibration of CH_2 groups. This peak occurred when the carbon atom from GMA was attached to the carbon atom from styrene as well as forming aliphatic carbons in the main chain and side chain of the copolymer [23]. Broader peak was observed at 1wt% and 2wt% of ST-co-GMA-clay (1.30E) nanocomposites which indicated stronger bonding between styrene and glycidyl methacrylate compared to other nanocomposites as shown in Figure 1(c-d) [21]. The C-O stretching vibration was observed due to the carbonyl group in the nanocomposites which showed the peak at 1150cm^{-1} [25]. The absorption peak at 1105cm^{-1} represented the Si-O-C asymmetric stretching mode in ring opening for styrene and glycidyl methacrylate. The intensity of this peak decreased when fumed silica and clay was added into the ST-co-GMA. This was due to the CH_3 groups attached to the Si-O-Si ring that filled the voids within ST-co-GMA [24]. The absorption peak at 1040cm^{-1} was assigned to Si-O-Si bonding in the nanocomposites that confirmed the bonding between the silica and clay (1.30E) [26]. IR spectra at 950cm^{-1} represented the small number of unreacted Si-CH_3 bonds existed within the nanocomposites [26]. 2wt% of clay (1.30E) showed less transmittance among all the nanocomposites that confirmed strong bonding with styrene, fumed silica and clay (1.30E) [27]. Therefore, it could be concluded that 2wt% of clay (1.30E) was more suitable to be incorporated into ST-co-GMA-fsi nanocomposites among all the nanocomposites.

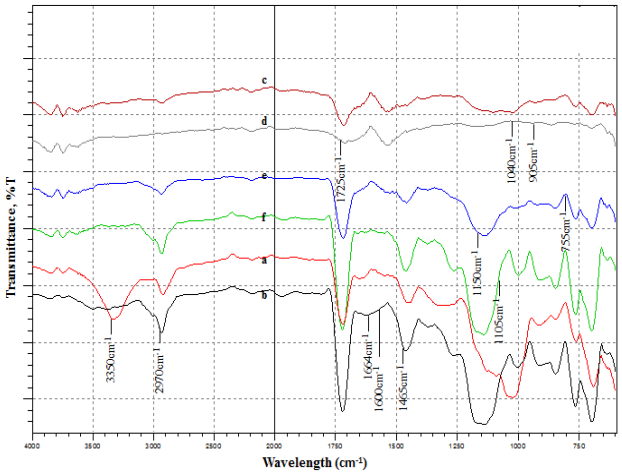

Figure 1 FT-IR spectra of (a) ST-co-GMA (b) ST-co-GMA-fsi nanocomposite (c) ST-co-GMA-fsi-clay (1.30E) nanocomposite, 1wt% (d) ST-co-GMA-fsi-clay (1.30E) nanocomposite, 2wt% (e) ST-co-GMA-fsi-clay (1.30E) nanocomposite, 3wt% (f) ST-co-GMA-fsi-clay (1.30E) nanocomposite, 4wt%

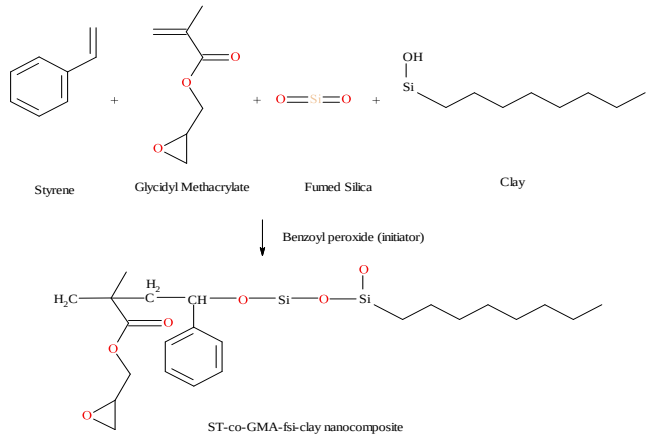

Figure 2 Schematic chemical reaction of ST-co-GMA-fsi-clay (1.30E) nanocomposites in the presence of benzoyl peroxide

3.2 Scanning Electron Microscopy (SEM)

Scanning electron microscopy (SEM) is used to explain the morphology of the ST-co-GMA, ST-co-

GMA-fsi and different weight loadings of clay loaded ST-co-GMA-fsi-clay (1.30E) nanocomposites.

The fracture surface of St-co-GMA was shown in Figure 3(a). This indicated the well interaction between styrene and glycidyl methacrylate [28]. ST-co-GMA-fsi nanocomposite showed moderately even surface that proved the nanocomposite was typically brittle as shown in Figure 3(b) [29]. This proved that silica improved the compatibility with ST-co-GMA by forming strong covalent bond. The nanocomposites showed uniform surface morphology due to the 1wt% and 2wt% of clay loading as shown in Figure 3(c-d). This occurred as the clay aggregates into small particles after polymerization and dispersed homogeneously into the ST-co-GMA-fsi [29]. Higher clay loading (3wt% and 4wt%) into ST-co-GMA-fsi would cause agglomeration as shown in Figure 3(e-f). This was due to clay loading over 2wt% prevented the intercalation mechanism and the properties of the material led to large agglomerate [30].

From the above observations, it could be concluded that there was a good compatibility as well as the well dispersion of 2wt% of clay (1.30E) into ST-co-GMA-fsi. The uniform surface of 2wt% of ST-co-GMA-fsi-clay (1.30E) nanocomposites proved the well interfacial bonding between clay and ST-co-GMA-fsi, as reflected in the mechanical and thermal properties.

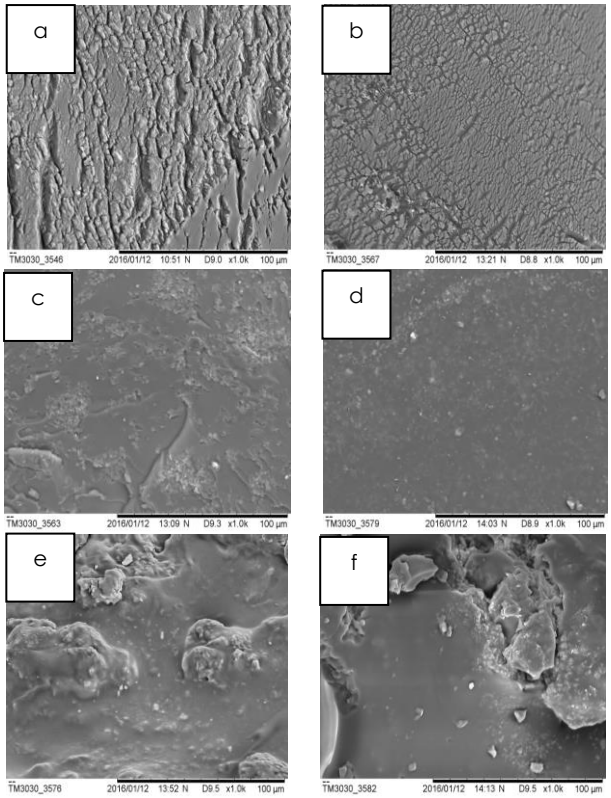

Figure 3 SEM micrographs of (a) ST-co-GMA (b) ST-co-GMA-fsi nanocomposite (c) ST-co-GMA-fsi-clay (1.30E) nanocomposite, 1wt% (d) ST-co-GMA-fsi-clay (1.30E) nanocomposite, 2wt% (e) ST-co-GMA-fsi-clay (1.30E) nanocomposite, 3wt% (f) ST-co-GMA-fsi-clay (1.30E) nanocomposite, 4wt%

3.3 Adsorption Isotherm

The N_2 adsorption isotherms for ST-co-GMA, ST-co-GMA-fsi, ST-co-GMA-fsi-clay (1.30E) nanocomposites were shown in Figure 4. Specific surface area (S_{BET}) was calculated by the Brunauer-Emmett-Teller (BET) equation [31].

2wt% of ST-co-GMA-fsi-clay (1.30E) nanocomposite showed a rather straight section, which extended up to P/P_o=0.55 whereas 1wt%, 3wt% and 4wt% of ST-co-GMA-fsi-clay (1.30E) nanocomposites showed extension up to P/P_o=0.43 as shown in Figure 4. ST-co-GMA and ST-co-GMA-fsi nanocomposite showed lowest extension, which was up to P/P_o=0.26. This proved that 2wt% of ST-co-GMA-fsi-clay (1.30E) nanocomposite had strong interfacial bonding that reduced the amount adsorbed on the nanocomposite.

The incorporation of silica into ST-co-GMA showed higher surface area and average pore volume compared to ST-co-GMA in Table 2. This showed that silica improved the interfacial bonding between styrene and glycidyl methacrylate. 2wt% of ST-co-GMA-fsi-clay (1.30E) nanocomposite had higher surface area and average pore volume with less pore size among all the nanocomposites. This was due to the uniform dispersion of clay particles in the nanocomposite which created strong interfacial interaction between the clay and ST-co-GMA-fsi up to 2wt% [32]. Higher clay loadings would reduce the strong interfacial interaction and thus the surface area and average pore volume decreased. The adsorption isotherms indicated that the pores were mesoporous. According to original IUPAC classification, the isotherm patterns of ST-co-GMA, ST-co-GMA-fsi, ST-co-GMA-fsi-clay (1.30E) nanocomposites were type IV isotherms [33].

Therefore, it proved that 2wt% of ST-co-GMA-fsi-clay (1.30E) nanocomposite had the highest surface area and average pore volume with less pore size, which was reflected in the surface morphology.

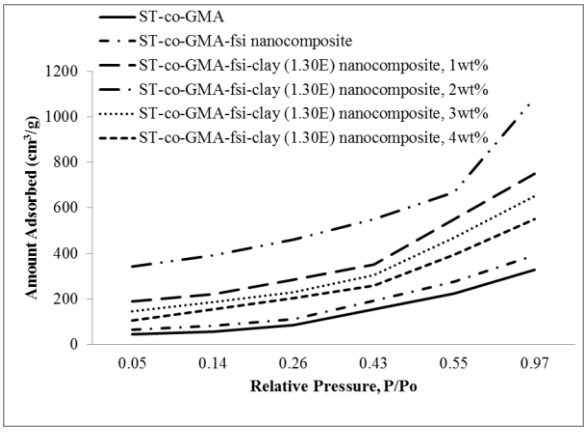

Figure 4 N_2 adsorption isotherms of ST-co-GMA, ST-co-GMA-fsi and ST-co-GMA-fsi-clay (1.30E) nanocomposites

Table 2 Physical properties detected from N_2 adsorption at 77K on ST-co-GMA, ST-co-GMA-fsi and ST-co-GMA-fsi-clay (1.30E) nanocomposites

Samples	Specific surface area, S_{BET}(m²/g)	Average pore volume, V_m (10^{-4}cm³/g)	d_{BET} (nm)	Type of isotherms
ST-co-GMA	238.29	8.07	1.94	IV
ST-co-GMA-fsi nanocomposite	254.23	8.41	1.57	IV
ST-co-GMA-fsi-clay (1.30E) nanocomposite, 1wt%	309.71	10.97	0.65	IV
ST-co-GMA-fsi-clay (1.30E) nanocomposite, 2wt%	318.52	11.82	0.63	IV
ST-co-GMA-fsi-clay (1.30E) nanocomposite, 3wt%	288.64	9.86	0.78	IV
ST-co-GMA-fsi-clay (1.30E) nanocomposite, 4wt%	282.56	9.73	0.81	IV

3.4 Tensile Properties

Tensile strength of ST-co-GMA, ST-co-GMA-fsi, ST-co-GMA-fsi-clay (1.30E) nanocomposites were presented in Figure 5. The tensile strength of the nanocomposites were increasing with the clay loading and reached a maximum at 2wt% of clay [34]. 1wt% and 2wt% clay loading particles filled the spaces between the ST-co-GMA-fsi chains, thus gave a rigid structure with better tensile strength value of 0.0524GPa and 0.0561GPa [35]. However, addition of clay decreased the strength as the agglomeration took place at higher clay content. The higher clay loadings such as 3wt% and 4wt% occurred aggregates in ST-co-GMA-fsi chains which weakened the bonds in the nanocomposites and thus the tensile strength decreased [36].

The tensile modulus of ST-co-GMA, ST-co-GMA-fsi, ST-co-GMA-fsi-clay (1.30E) nanocomposites in Figure 6. 2wt% of ST-co-GMA-fsi-clay (1.30E) nanocomposite showed the highest tensile modulus compared to ST-co-GMA, ST-co-GMA-fsi, 1wt%, 3wt% and 4wt% of ST-co-GMA-fsi-clay (1.30E) nanocomposites. The clay particles at low loading (1wt% and 2wt%) were easily dispersed within ST-co-GMA-fsi due to the small size of the particles and therefore, the tensile modulus of the nanocomposites increased [37]. However, the increase in quantity of clay reduced the tensile modulus. This was due to the heterogeneous distribution of the clay with ST-co-GMA that led to the agglomeration of clay particles within the nanocomposites. Once the filler loading increased, it tended to agglomerate and formed phase segregation of the nanocomposite. Once the phase segregation became higher, the particle-particle contact was reduced and this led to lower poor interfacial bonding. Therefore, the nanocomposite could not withstand higher force and thus, the tensile modulus was decreased [38].

It was concluded that 2wt% of clay (1.30E) provided the best tensile strength and tensile modulus improvement into ST-co-GMA-fsi nanocomposite. This confirmed that clay (1.30E) at low loading provided better interfacial bonding and compatibility toward the ST-co-GMA-fsi.

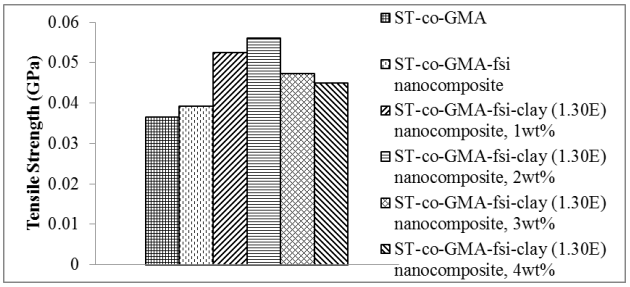

Figure 5 Tensile strength of ST-co-GMA, ST-co-GMA-fsi and ST-co-GMA-fsi-clay (1.30E) nanocomposites

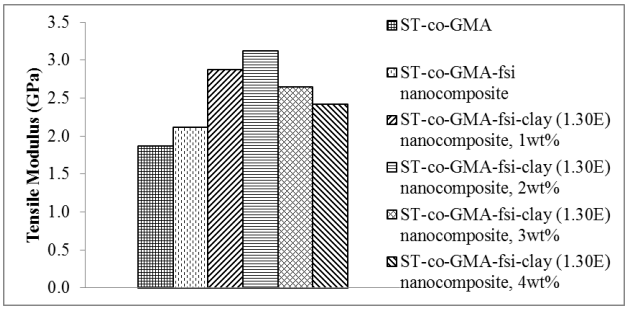

Figure 6 Tensile modulus of ST-co-GMA, ST-co-GMA-fsi and ST-co-GMA-fsi-clay (1.30E) nanocomposites

3.5 Thermogravimetric Analysis (TGA)

The thermal stability of ST-co-GMA, ST-co-GMA-fsi and ST-co-GMA-fsi-clay (1.30E) nanocomposites were shown in Figure 7. The thermal stability of ST-co-GMA-fsi-clay (1.30E) nanocomposites were significantly higher compared to ST-co-GMA and ST-co-GMA-fsi nanocomposites.

The nanocomposites were thermally degraded in two stages. The first step of the thermal decomposition is occurred at about 310°C to 380°C due to the broken bond of organo clay cations that accessible to oxygen [39]. This occurred at the end chain of the ST-co-GMA followed by random chain scissions [40]. Based on the TGA thermograph, the weight loss was 3.8%, 3.0%, 2.5%, 2.3%, 2.7% and 2.9% for ST-co-GMA, ST-co-GMA-fsi and various weight percentage of clay loaded ST-co-GMA-fsi-clay (1.30E) nanocomposites respectively. The second thermal degradation occurred as the cations adsorbed in the interlayer were oxidised in the range of 480°C to 700°C [39]. The weight loss of ST-co-GMA, ST-co-GMA-fsi and various weight percentage of clay loaded ST-co-GMA-fsi-clay (1.30E) was 96.1%, 94.7%, 86.1%, 84.8%, 87.7% and 92.3%. From the two thermal degradation, it showed that ST-co-GMA-fsi-clay (1.30E) nanocomposites started the thermal degradation at a higher temperature relative to ST-co-GMA-fsi nanocomposite and ST-co-GMA. This was due to the the degradation temperature of silica at 360°C that led to fast thermal degradation on ST-co-GMA-fsi nanocomposite. For ST-co-GMA, the thermal degradation started at lower temperature among all the nanocomposites as it had weak covalent bonds between styrene and glycidyl methacrylate [41]. Therefore, the incorporation of clay (1.30E) improved the interfacial bonding and thus improved the thermal stability of the nanocomposite, as proven by SEM result.

The activation energy of ST-co-GMA, ST-co-GMA-fsi and ST-co-GMA-fsi-clay (1.30E) nanocomposites were calculated using Arrhenius equation [42]. The activation energy of ST-co-GMA-fsi-clay (1.30E) nanocomposites were significantly higher than that of ST-co-GMA and ST-co-GMA-fsi nanocomposite in Table 3. This showed that clay loaded nanocomposites had greater thermal stability. Overall, 2wt% of clay (1.30E) was compatible to be incorporated into ST-co-GMA-fsi nanocomposite to enhance the thermal properties.

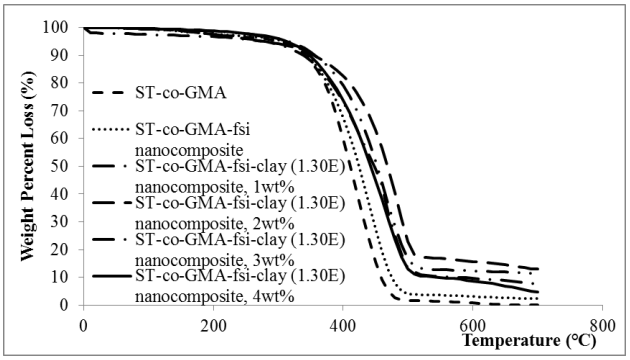

Figure 7 TGA curves of ST-co-GMA, ST-co-GMA-fsi and ST-co-GMA-fsi-clay (1.30E) nanocomposites

Table 3 Activation energy of ST-co-GMA, ST-co-GMA-fsi and ST-co-GMA-fsi-clay (1.30E) nanocomposites

Samples	Temperature (°C)		Weight (%)		Activation Energy , E_a (kJ/mol)
ST-co-GMA	T_i[a]	244.5	W_{Ti}[d]	96.2	40.9
	T_m[b]	492.5	W_{Tm}[e]	1.8	
	T_f[c]	648.7	W_{Tf}[f]	0.1	
ST-co-GMA-fsi nanocomposite	T_i[a]	246.8	W_{Ti}[d]	97.0	43.4
	T_m[b]	493.5	W_{Tm}[e]	4.7	
	T_f[c]	693.5	W_{Tf}[f]	2.3	
ST-co-GMA-fsi-clay (1.30E) nanocomposite, 1wt%	T_i[a]	249.5	W_{Ti}[d]	97.5	67.1
	T_m[b]	500.0	W_{Tm}[e]	17.0	
	T_f[c]	693.5	W_{Tf}[f]	11.4	
ST-co-GMA-fsi-clay (1.30E) nanocomposite, 2wt%	T_i[a]	250.5	W_{Ti}[d]	97.7	68.9
	T_m[b]	501.2	W_{Tm}[e]	22.3	
	T_f[c]	693.5	W_{Tf}[f]	12.9	
ST-co-GMA-fsi-clay (1.30E) nanocomposite, 3wt%	T_i[a]	248.5	W_{Ti}[d]	97.3	54.9
	T_m[b]	495.6	W_{Tm}[e]	15.8	
	T_f[c]	693.5	W_{Tf}[f]	9.6	
ST-co-GMA-fsi-clay (1.30E) nanocomposite, 4wt%	T_i[a]	247.2	W_{Ti}[d]	97.1	50.1
	T_m[b]	495.2	W_{Tm}[e]	14.9	
	T_f[c]	693.5	W_{Tf}[f]	4.8	

[a]Temperature corresponding to the maximum rate of mass loss
[b]Temperature corresponding to the beginning of decomposition
[c]Temperature corresponding to the end of decomposition
[d]Mass loss at temperature corresponding to the maximum rate of mass loss
[e]Mass loss at temperature corresponding to the beginning of decomposition
[f]Mass loss at temperature corresponding to the end of decomposition

3.6 Moisture Absorption Analysis

The moisture absorption of ST-co-GMA, ST-co-GMA-fsi and ST-co-GMA-fsi-clay (1.30E) nanocomposites were clearly shown in Figure 8. ST-co-GMA showed a sharp increment of moisture absorption at the first 10 minutes and it remained constant after 50 minutes. ST-co-GMA-fsi and various clay loading of ST-co-GMA-fsi-clay (1.30E) nanocomposites showed the same moisture absorption pattern with a gradual increment up to 60 minutes.

ST-co-GMA showed the highest moisture absorption due to the less entanglement of molecules on both side of the interface thus, weak interfacial bonding were formed between styrene and glycidyl methacrylate. Silica had improved the adhesion with ST-co-GMA that decreased the moisture absorption ability by reducing the water diffusion pathway [41]. Stronger adhesion within the nanocomposites created strong interfacial bonding that improved the particle-particle interaction. This interaction reduced the pores within the nanocomposites and thus, more water was resist to be diffused into the nanocomposite. Incorporation of clay generated better tortuous pathway and increased the barrier property for water diffusion within the nanocomposites compared to incorporation of silica. Clay (1.30E) acted as barriers to the hindrance of the moisture into the ST-co-GMA-fsi [43]. 1wt% and 2wt% of ST-co-GMA-fsi-clay (1.30E) nanocomposites showed lower moisture absorption (<0.5%) among all the nanocomposites. This was due to the nano sized clay particle penetrated into the ST-co-GMA-fsi with strong interfacial bonding that reduced the ability of water absorption through the nanocomposite structure [44]. Higher clay loadings (3wt% and 4wt%) created lots of tiny in-between spaces due to excessive clays within the nanocomposites which created abundant surface area that allowed water molecules to enter the nanocomposites [45].

Throughout this study, 2wt% of ST-co-GMA-fsi-clay nanocomposites had significantly reduced the diffusion of moisture into the nanocomposites and enhanced the compatibility between clay (1.30E) and ST-co-GMA-fsi.

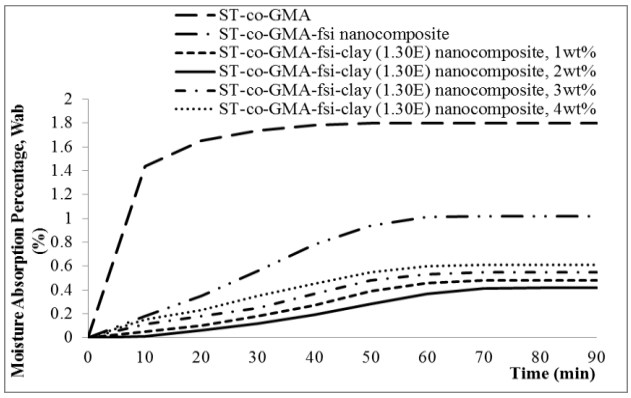

Figure 8 Moisture absorption curves of ST-co-GMA, ST-co-GMA-fsi and ST-co-GMA-fsi-clay (1.30E) nanocomposites

4.0 CONCLUSION

From the present study, the followings can be concluded:

(a) ST-co-GMA-fsi-clay (1.30E) nanocomposites were prepared via free radical polymerization.

(b) ST-co-GMA-fsi bonding and fsi-clay bonding were confirmed by Si-O-C and Si-O-Si peaks in FT-IR spectroscopy.

(c) From the surface morphology, it was found that the dispersion of 2wt% of clay (1.30E) significantly enhanced the compatibility of the nanocomposites.

(d) From the surface analysis, it proved that the 2wt% of ST-co-GMA-fsi-clay (1.30E) nanocomposite had higher surface area and pore volume with less pore size compared to ST-co-GMA and other nanocomposites.

(e) The tensile strength and modulus of 2wt% of ST-co-GMA-fsi-clay (1.30E) nanocomposite was the highest which confirmed the best compatibility of clay (1.30E) into ST-co-GMA-fsi nanocomposite.

(f) 2wt% of clay (1.30E) improved the thermal stability significantly due to the strong interfacial bonding within the nanocomposite.

(g) The strong interfacial bonding formed in 2wt% of ST-co-GMA-fsi-clay (1.30E) nanocomposite led to higher water resistance. It was concluded that 2wt% of ST-co-GMA-fsi-clay (1.30E) nanocomposite enhanced the physical, morphological and mechanical properties as well as thermal stability.

Acknowledgement

This research is fully supported by PhD Student grant, F02 (DPP40)/1260/2015(15) and Ministry of Education Malaysia Grant, FRGS/SG02(01)/1085/2013(31). The authors fully acknowledged Universiti Malaysia Sarawak for the approved fund which makes this important research viable and effective.

References

[1] Hanifah, S. A., Hamzah, N. and Heng, L. Y. 2013. Microspheres Poly(Glycidyl Methacrylate-co-Styrene) by Photopolymerization, Sains Malaysiana. *Rapid Synthesis of Magnetic*. 42(4): 487-493. http://www.ukm.my/jsm/pdf_files/SM-PDF-42-4-2013/09%20Sharina%20Abu%20Hanifah.pdf.

[2] Chen, C. H. and Lee, W. C. 2001. Affinity Chromatography of Protein on Nonporous Copolymerized Particles of Styrene, Methyl Methacrylate and Glycidyl Methacrylate. *Journal of Chromatography A*. 921(1): 31-37. DOI: 10.1016/S0021-9673(01)00712-9.

[3] Chung, T. H., Pan, H. C. and Lee, W. C. 2007. Preparation and Application of Magnetic Poly (Styrene-Glycidyl Methacrylate) Microspheres. *Journal of Magnetism and Magnetic Materials*. 311(1): 36-40. DOI: 10.1016/j.jmmm.2006.11.165.

[4] Zanchet, A., Carli, L. N., Giocanela, M., Brandalise, R. N. and Crespo, J. S. 2012. Use of Styrene Butadiene Rubber Industrial Waste Devulcanized by Microwave in Rubber Composites for Automotive Application. *Materials Design*. 39: 437-443. DOI: 10.1016/j.matdes.2012.03.014.

[5] Clemons, D. and Tristan. 2013. *Applications of Multifunctional Poly(Glycidyl Methacrylate) (PGMA) Nanoparticles in Enzyme Stabilization and Drug Delivery*. Australia: The University of Western Australia. http://research-repository.uwa.edu.au/en/publications/applications-of-multifunctional-polyglycidyl-methacrylate-pgma-nanoparticles-in-enzyme-stabilization-and-drug-delivery(56ca7d2a-cb03-4fc0-830b-f206529a4413).html.

[6] Kunita, M. H., Girotto, E. M., Muniz, E. C. and Rubira, A. F. 2006. Polypropylene Grafted with Glycidyl Methacrylate using Supercritical CO_2 Medium. *Brazilian Journal of Chemical Engineering*. 23(2): 267-271. DOI: 10.1590/S0104-66322006000200015.

[7] Wei, L., Hu, N. and Zhang, Y. 2010. Synthesis of Polymer-Mesoporous Silica Nanocomposites. *Materials*. 3(7): 4066-4079. http://www.mdpi.com/1996-1944/3/7/4066.

[8] Grim, R. E. 1968. *Clay Mineralogy*. New York: McGraw-Hill. https://www.amazon.com/Clay-Mineralogy-R-Grim/dp/0070248362.

[9] Conzatti, L. 2012. The Clay Mineral Modifier as the Key to Sheer the Properties of Rubber Nanocomposites. *Applied Clay Science*. 61: 14-21. DOI: 10.1016/j.clay.2012.03.004

[10] Kim, K., Seo, B., Lee, J. Y., Choi, B. J., Kwag, G. H., Paik, H. J. and Kim, W. 2015. Reduced Filler Flocculation in the Silica-filled Styrene-Butadiene-Glycidyl Methacrylate Terpolymer. *Composites Interfaces*. 22(2): 137-149. DOI: 10.1080/15685543.2015.997115.

[11] Yin, C., Zhang, Q. and Gong, D. 2013. Preparation and Properties of Silica/Styrene Butadiene Rubber Masterbatches by Latex co-Coagulating Technology. *Polymer Composites*. 35(6): 1212-1219. DOI: 10.1002/pc.22770.

[12] Barrantes, I. M., Valentin, J. L., Rodriquez, A., Garrido, I. Q. and Paris, R. 2012. Poly(Styrene)/Silica Hybrid Nanoparticles Prepared via ARTP as High Quality Fillers in Elastomeric Composites. *Journal of Materials Chemistry*. 22(4): 1403-1410. DOI: 10.1039/C1JM14295J.

[13] Ou, B., Yang, G., Xiao, Y., Zeng, X., Zhou, Z., Liu, Q., Zhang, X. and Li, D. 2013. Covalent Functionalization of Silica Nanoparticle with Poly(Glycidyl Methacrylate) via ATRP at Ambient Temperature. *Journal of Macromolecular Science Part A*. 50(1): 25-28. DOI: 10.1080/10601325.2013.735948.

[14] Nemati, N., Taromi, F. A. and Mirzataheri, M. 2015. In-situ Water Based Emulsion Copolymerization of Styrene/Ethylhexyl Acrylate in Presence of Cloisite 15A. *Procedia Materials Science*. 11: 542-547. DOI: 10.1016/j.mspro.2015.11.046.

[15] Devi, R. R. and Maji, T. K. 2013. In Situ Polymerized Wood Polymer Composite: Effect of Additives and Nanoclay on the Thermal, Mechanical Properties. *Materials Research Bulletin*. 16(4): 954-963. http://www.scielo.br/scielo.php?script=sci_arttext&pid=S1516-14392013000400035.

[16] Bokobza, L., Leroy, E. and Lalanne, V. 2009. Effect of Filling Mixtures of Sepiolite and A Surface Modified Fumed Silica on the Mechanical and Swelling Behavior of a Styrene-Butadiene Rubber. *European Polymer Journal*. 45(4): 996-1001. DOI: 10.1016/j.eurpolymj.2008.12.028.

[17] Devi, R. R. and Maji, T. K. 2013. Interfacial Effect of Surface Modified TiO_2 and SiO_2 Nanoparticles Reinforcement in the Properties of Wood Polymer Clay Nanocomposites. *Journal of the Taiwan Institute of Chemical Engineers*. 44(4): 505-514. DOI: 10.1016/j.jtice.2012.11.018

[18] Ogunsona, E., Ogbomo, S., Nar, M. and D'Souza, N. A. 2011. Thermal and Mechanical Effects in Polystyrene-Montmorillonite Nanocomposite Foams. *Cellular Polymers*. 30(2): 79-84.

[19] Lai, J. C. H., Rahman, M. R. and Hamdan, S. 2015. Physical, Mechanical, and Thermal Analysis of Polylactic Acid/Fumed Silica/Clay (1.28E) Nanocomposites. *International Journal of Polymer Science*. 2015: 1-8. DOI: 10.1155/2015/698738.

[20] Yang, W., Dominici, F., Fortunati, E., Kenny, J. M. and Puglia, D. 2015. Melt Free Radical Grafting Of Glycidyl Methacrylate (GMA) Onto Fully Biodegradable Poly(Lactic) Acid Films: Effect of Cellulose Nanocrystals And A Masterbatch Process. *RSC Advances*. 5(41): 32350-32357. DOI: 10.1039/C5RA00894H.

[21] Sowribabu, K., Reddy, A. R. C., Sujatha, C. and Reddy, K. V. 2011. Structural and Optical Properties of ZnO Nanoclusters Supported on Mesoporous Silica. *Journal of Optoelectronics and Advanced Materials*. 5(9): 943-947. https://www.researchgate.net/publication/286797171_Structural_and_optical_properties_of_ZnO_nanoclusters_supported_on_mesoporous_silica.

[22] Mukasa-Tebandeke, I. Z., Ssebuwufy, P. J. M., Nyanzi, S. A., Schumann, A., Nyakairu, G. W. A., Ntale, M. and Lugolobi, F. 2015. The Elemental, Mineralogical, IR, DTA and XRD Analyses Characterized Clays and Clay Minerals of Central and Eastern Uganda. *Advances in Materials Physics and Chemistry*. 5(2): 67-86. DOI: 10.4236/ampc.2015.52010.

[23] Bicak, N., Bulutcu, N., Senkal, B. F. and Gazi, M. 2001. Modification of Crosslinked Glycidyl Methacrylate-based Polymers for Boron-Specific Column Extraction. *Reactive and Functional Polymers*. 47(3): 175-184. DOI: 10.1016/S1381-5148(01)00025-6.

[24] Sultan, M. T., Rahman, M. R., Hamdan, S., Lai, J. C. H. and Talib, Z. A. 2016. Clay Dispersed Styrene-co-Glycidyl Methacrylate Impregnated Kumpang Wood Polymer Nanocomposites: Impact on Mechanical and Morphological Properties. *BioResources*. 11(3): 6649-6662. http://ojs.cnr.ncsu.edu/index.php/BioRes/article/view/BioRes_11_3_6649_Tipu_Sultan_Clay_Dispersed_Styrene_Methacrylate_Kumpang_Wood.

[25] Bellamy, L. J. 1975. *The Infra-Red Spectra of Complex Molecules*. London: Chapman and Hall Ltd. http://link.springer.com/book/10.1007%2F978-94-011-6520-4.

[26] Jing, S. Y., Lee, H. J. and Choi, C. K. 2002. Chemical Bond Structure on Si-O-C Composite Films with a Low Dielectric Constant Deposited by Using Inductively Coupled Plasma Chemical Vapour Deposition. *Journal of Korean Physical Society*. 41(5): 769-773. http://scholar.ndsl.kr/schArticleDetail.do?cn=NART14756627.

[27] Alizadeh, D. 2016. *Effect of Clay Addition on Mode II Interlaminar Fracture Toughness and Flexural Fatigue Behavior of Glass/Epoxy Composites*. Canada: Concordia University. http://spectrum.library.concordia.ca/981282/1/Alizadeh_MASc_F2016.pdf.

[28] Lv, J. N., Fang, S. J. and Chen, L. 2009. Preparation and Characterization of Affinity Polymer Basic Microspheres by Soap-Free Emulsion Polymerization. *Chinese Journal of Polymer Science*. 27(1): 101-108. http://www.cjps.org/EN/Y2009/V27/I1/101.

[29] Wang, H. T., Zhong, W., Xu, P. and Du, Q.G. 2004. Properties of Polyimide/Silica Nanohybrids from Silicic Acid Oligomer. *Macromolecular Materials and Engineering*. 289(9): 793-799. DOI: 10.1002/mame.200400002.

[30] Fan, J., Liu, S., Chen, G. and Qi, Z. 2002. SEM Study of a Polystyrene/Clay Nanocomposite. *Journal of Applied Polymer Science*. 83(1): 66-69. DOI: 10.1002/app.2232.

[31] Flitz, C. 2008. *Preparation and Characterization of Recycled Polypropylene Based Nanocomposites*. Turkey: Middle East Technical University. http://citeseerx.ist.psu.edu/viewdoc/download?doi=10.1.1.632.7227&rep=rep1&type=pdf.

[32] Brunauer, B., Emmett, P. H. and Teller, E. 1938. Adsorption of Gases in Multimolecular Layers. *Journal of the American Chemical Society*. 60(2): 309-319. DOI: 10.1021/ja01269a023.

[33] Hazarika, A. and Maji, T. K. 2014. Modification of Softwood by Monomers and Nanofillers. *Defence Science Journal*. 64(3): 262-272. DOI: 10.14429/dsj.64.7325.

[34] Surej, R. C., Praseetha, P. N. and George, K.E. 2011. In Situ Addition Polymerization of Styrene using Nanoclay and Evaluation of Properties. *International Journal of Applied Science and Engineering*. 1(4): 133-135. http://www.ijera.com/papers/Vol2_issue4/FT2410451049.pdf.

[35] Ahmed, J. K., Al-maamori, M. H. and Ali, H.M. 2015. Effect of Nano Silica on the Mechanical Properties of Styrene-Butadiene Rubber (SBR) Composite. *International Journal of Materials Science and Applications*. 4(2-1): 15-20. DOI: 10.11648/j.ijmsa.s.2015040201.14.

[36] Abbas, F. and Al-Husnawi, H. 2014. *A Study of the Effect of Zinc Oxide on Physical Properties of NR/SBR Blends*. Iraq: University of Kufa. http://www.iasj.net/iasj?func=fulltext&aId=102860.

[37] Chang, C. R. and Chang, F.C. 1996. Polymer Blends of Polyamide-6 and Poly(Phenylene Oxide) Compatibilized by Styrene-co-Glycidyl Methacrylate. *Journal of Applied Polymer Science*. 61(13): 2411-2421. DOI: 10.1002/(SICI)1097-4628(19960926)61:13<2411::AID-APP21>3.0.CO;2-5.

[38] Azizi Samir, M. A. S., Alloin, F., Dufrense, A. 2005. Review of Recent Research into Cellulosic Whiskers, Their Properties and Their Application in Nanocomposite Field. *Biomacromolecules*. 6(2): 612-626. DOI: 10.1021/bm0493685.

[39] Ramachandran, V. S. and Kacker, K. P. 1964. The Thermal Decomposition of Dye-clay Mineral Complexes. *Journal of Chemical Technology and Biotechnology*. 14(10): 455-460. DOI: 10.1002/jctb.5010141008.

[40] Jiang, S., Deng, J. and Yang, W. 2008. Block Copolymers Prepared by Free Radical Polymerization using a-Methylstyrene-containing Precopolymer as Macroinitiator. *Polymer Journal*. 40: 543-548. DOI: 10.1295/polymj.PJ2007192.

[41] Liang, S. J. and Yang, W. T. 2011. Functionalization of Polypropylene and Compatibilization of Polypropylene/nylon 6 Blends with Copolymers Containing a-methyl Styrene Units. *Acta Polymerica Sinica*. 11(2): 180-185. https://www.degruyter.com/view/j/epoly.2010.10.issue-1/epoly.2010.10.1.1033/epoly.2010.10.1.1033.xml.

[42] Chanmal, C. V. and Jog, J. P. 2008. Dielectric Relaxations in PVDF/$BaTiO_3$ Nanocomposites. *eXPRESS Polymer Letters*. 2(4): 294-301. DOI: 10.3144/expresspolymlett.2008.35.

[43] Zeng, Z., Yu, J. and Guo, Z. X. 2004. Preparation of Epoxy-Functionalized Polystyrene/Silica Core-Shell Composite Nanoparticles. *Journal of Polymer Science*. 42(9): 2253-2262. DOI: 10.1002/pola.20059.

[44] Rozman, H. D., Kumar, R. N., Abusamah, A. and Saad, M. J. 1998. Miscibility between Natural Rubber and Tackifiers. II. Phase Diagrams of the Blends of Natural Rubber and Petroleum Resins. *Journal of Applied Polymer Science*. 67(2): 221-229. DOI: 10.1002/(SICI)1097-4628(19980110)67:2<221::AID-APP4>3.0.CO;2-W.

[45] Barshad, I. 1952. Adsorptive and Swelling Properties of Clay-Water System. *Clay Clay Minerals*. 1(1): 70-77. DOI: 10.1346/CCMN.1952.0010108.